Journal of Alloys and Compounds 509 (2011) 8620–8624

Contents lists available at ScienceDirect

Journal of Alloys and Compounds

journal homepage: www.elsevier.com/locate/jallcom

N-doped carbon nanotubes synthesized in high yield and decorated with CeO_2 and SnO_2 nanoparticles

Rui Zhang, Li Li, Lei Chen, Guo Zhang, Keying Shi*

Key Laboratory of Functional Inorganic Material Chemistry, Ministry of Education, Key Laboratory of Physical Chemistry, School of Chemistry and Chemical Engineering, Heilongjiang University, Harbin 150080, People's Republic of China

ARTICLE INFO

Article history:
Received 6 May 2011
Received in revised form 11 June 2011
Accepted 13 June 2011
Available online 21 June 2011

Keywords:
Nitrogen doped
Carbon nanotubes
Composite
NO electrooxidation

ABSTRACT

Nitrogen doped multiwalled carbon nanotubes (CN_xNTs) with high yield and purity have been successfully prepared from *n*-propylamine precursor with $Co_xMg_{1-x}MoO_4$ catalyst. The maximum yield of the CN_xNTs is 920%. SnO_2 and CeO_2 nanoparticles are decorated on the surface of CN_xNTs without any acid treatment due to the inherent interface activity. The TEM images reveal that SnO_2 and CeO_2 nanoparticles were anchored on the surface of the CN_xNTs uniformly, and the XPS results indicate that the doped nitrogen atoms of CN_xNTs play significant roles in immobilizing SnO_2 and CeO_2 nanoparticles, and the mechanism of the composite process has been discussed. The electrooxidation performance of the composites for NO at the modified electrodes was investigated. The CN_xNTs-based composites show greater activity and sensitivity than the conventional CNTs-based composites for NO electrooxidation, which render them excellent electrode materials for NO detection and other potential applications.

1. Introduction

The unique structure and the excellent properties of carbon nanotubes (CNTs) have attracted tremendous attention of a large number of researchers. CNTs can be used as special nanoscale semiconductor devices, hydrogen storage materials, electronic and sensor materials, etc. [1–8]. Recently, the study of CNTs-based composites is becoming a promising and challenging area of research owing to their potential applications [9–15].

Doping nitrogen atoms during the growth process is another promising approach to improve the electronic properties of CNTs. Nitrogen atom has one more electron than carbon atom, so the CN_xNTs may show the performance of N-type semiconductor for the extra electron acted as the current carrier [16]. To a large extent, the electronic properties of CN_xNTs are determined by the concentration of doped nitrogen, and through regulating the preparation condition, the concentration of doped nitrogen of CN_xNTs would be well-controlled. Wang and co-workers synthesized CN_xNTs with a nitrogen-doping level as high as 20 atomic % (at. %) [17]. However, the yield ratio is not ideal. Tao et al. obtained the CN_xNTs with high weight ratio but low nitrogen concentration of 0.6–3.2 at. % [18].

As the surface of CNTs is chemically inert, to fabricate CNTs-based composites, the CNTs are typically treated via harsh processes for activation by refluxing in concentrated acids, which destroys the π conjugation and reduces the conductance of the CNTs base [19]. The surface layer of CN_xNTs will present negative electricity due to the extra electron of the nitrogen atom. Employing CN_xNTs without any pre-treatment to composite with the functional materials directly is a promising method because the CN_xNTs can also be synthesized easily. Moreover, nitrogen atoms in the framework of CN_xNTs will form chemically active points which are available for metal or metallic oxide nanoparticles anchoring. Ghosh prepared ZnO/CN_xNTs composites via a simple wet-chemical method and studied their field emission performance [19]. Yue and co-workers obtained Pt/CN_xNTs composites which presented obvious catalytic activity for methanol oxidation [20].

Recently, SnO_2 has emerged as the NO_x sensor material. Espinosa and co-workers synthesized SnO_2/MWCNTs composites which present excellent sensitivity towards NO_x when operated at room temperature [21]. Topoglidis prepared the composites of SnO_2 and hemoglobin as electrode materials of NO electrochemical sensor [22]. It is well known that CeO_2 has been intensively studied for its utilization as three-way catalyst in automotive catalytic converter. The applications generally made use of the excellent redox property and oxygen storage capacity of CeO_2 [23]. Atribak studied the catalytic activity towards the oxidation of NO to NO_2 by using ceria-zirconia mixed oxides [24]. Thus, preparing SnO_2/CN_xNTs and CeO_2/CN_xNTs composites and investigating their NO electrooxidation property are very meaningful.

In this paper, the experiments for synthesizing high yield (yield = the mass of the products/the mass of the catalysts × 100%) CN_xNTs were carried out. The CN_xNTs with highest yield was obtained by pyrolysis of $Co_xMg_{1-x}MoO_4$ catalyst and *n*-propylamine feedstock at 900 °C with NH_3 flow rate of 300 mL/min.

* Corresponding author. Tel.: +86 451 86609141; fax: +86 451 86609141.
E-mail address: shikeying2008@yahoo.cn (K. Shi).

0925-8388/$ – see front matter © 2011 Elsevier B.V. All rights reserved.
doi:10.1016/j.jallcom.2011.06.051

This product has been employed to composite with SnO_2 and CeO_2 nanoparticles via a simple wet-chemical method, and the morphology and the mechanism of the composite process are presented. The application of SnO_2/CN_xNTs and CeO_2/CN_xNTs composites for detecting NO in the KH_2PO_4–NaOH buffer solution (PBS) saturated with NO was investigated by cyclic voltammetry (CV) and electrochemical impedance spectroscopy (EIS).

2. Experimental

2.1. Material preparation

At first, two series of CN_xNTs were synthesized via chemical vapor deposition method using Fe/MgO and $Co_xMg_{1-x}MoO_4$ as catalysts respectively. The Fe/MgO catalyst was obtained from 3.0 g $Mg(NO_3)_2{\cdot}6H_2O$, 1.2 g $C_6H_8O_7{\cdot}H_2O$ and 0.3 g $Fe(NO_3)_3{\cdot}9H_2O$ which dissolved in 10 mL H_2O, and then, the mixed solution stirred for 6 h at 85 °C, dried and calcined for 2 h at 450 °C in air. The $Co_xMg_{1-x}MoO_4$ catalyst was synthesized by an extremely efficient method [18]. The series using Fe/MgO as catalyst was carried out utilizing pyridine (C_5H_5N), 1, 2-ethylenediamine ($C_2H_8N_2$) and *n*-propylamine (C_3H_9N) as C and N feedstock respectively at 900 °C with NH_3 flow rate of 300 mL/min for 30 min. The samples were denoted as Fe-C_5-300, Fe-C_2-300, and Fe-C_3-300, respectively. The other series by using $Co_xMg_{1-x}MoO_4$ as catalyst was carried out by using *n*-propylamine (C_3H_9N) as feedstock, and was prepared in tube furnace at 900 °C for 30 min with NH_3 flow rates of 150, 300, 450 and 600 mL/min respectively. The samples were denoted as CoMo-150, CoMo-300, CoMo-450 and CoMo-600.

SnO_2/CN_xNTs composites were prepared from 30 mg CN_xNTs which dispersed in 40 mL distilled water by ultrasonication. Then 0.7 mL HCl and 1.0 g $SnCl_2{\cdot}2H_2O$ were added under vigorous stirring. The black suspension was further stirred for 2 h at room temperature, then filtrated and washed with distilled water repeatedly, and dried at 70 °C.

CeO_2/CN_xNTs composites were prepared from 100 mg CN_xNTs which dispersed in a 0.05 g/mL $Ce(NO_3)_3$ solution with ultrasonic radiation for 60 min at room temperature. Then, with vigorous stirring, 0.005 g/mL NaOH solution was added dropwise into the solution until the pH value was 10, washed repeatedly and dried at 60 °C.

SnO_2/CNTs and CeO_2/CNTs composites were prepared via the same method, and the CNTs (multi-walled carbon nanotubes) were first refluxed in a 30% nitric acid at 140 °C for 24 h. Employing the same method without compositing with CNTs and CN_xNTs, SnO_2 and CeO_2 nanoparticles were also prepared.

2.2. Material characterization

The morphological characterization of the CN_xNTs and the composites was carried out using scanning electron microscopy (SEM, Hitachi S-4800) with an acceleration voltage of 5 kV and transmission electron microscopy (TEM, JEOL-2100) with an acceleration voltage of 200 kV. The elements were quantified by X-ray photoelectron spectroscopy (XPS, VG ESCALAB 250). In addition, the configurations of nitrogen atom were confirmed by XPS excited by an X-ray source of Mg Kα (hm < 1253.6 eV) in an ultrahigh vacuum chamber with a base pressure of $<2 \times 10^{-8}$ Torr.

2.3. Electrochemical experiments

The activity of NO electrooxidation on the modified glassy carbon (GC) electrodes was studied. The preparation of the modified electrodes and the process of their electrochemical experiment were the same as those of single-walled carbon nanotube modified electrode, reported in our previous paper [25]. The electrochemical measurements were performed in a conventional three-electrode cell controlled with CHI660D electrochemical workstation (Beijing, China) and IM6e impedance measurement unit (ZAHNER Elektrik, Germany) with a Pt sheet and a saturated Ag/AgCl electrode as the counter and reference electrodes, respectively.

3. Results and discussion

Fig. 1 shows the experimental results about the yield ratio of two series of Fe/MgO and $Co_xMg_{1-x}MoO_4$ catalysts. Here, all the above experiments were carried out by maintaining a constant reaction time of 30 min. The results show that the sample with the highest yield ratio in the Fe/MgO series is the sample of Fe-C_3-300, and the yield ratio is about 460%, which reveals that C_3H_9N is easier for growing CN_xNTs than C_5H_5N and $C_2H_8N_2$. Then, the high efficient catalyst of $Co_xMg_{1-x}MoO_4$ and the feedstock of C_3H_9N were used to synthesize CN_xNTs with NH_3 flow rate range from 150 to 600 mL/min. As shown in Fig. 1, the obtained sample of CoMo-300 has the highest yield ratio of 920%. The optimalizing condition of

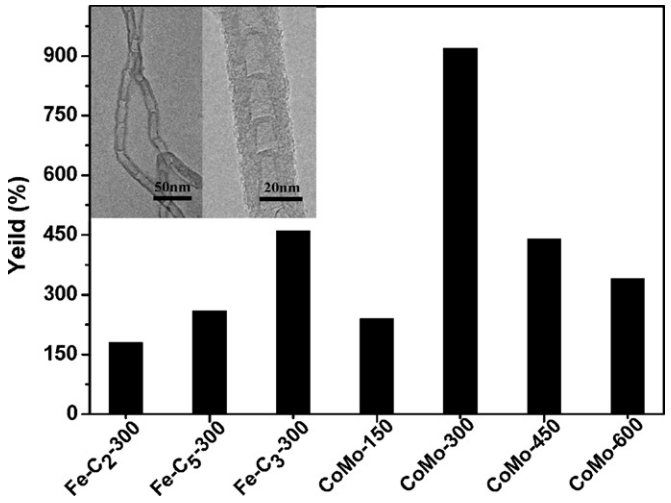

Fig. 1. The yield ratio versus histogram of the various products. The inset shows the TEM images of the sample of CoMo-300 (Catalyst: $Co_xMg_{1-x}MoO_4$; feedstock: C_3H_9N; reaction temperature: 900 °C; flow rate: 300 mL/min; reaction time: 30 min).

NH_3 flow rate for synthetizing high yield CN_xNTs is 300 mL/min. Henceforth the products of CoMo-300 were utilized for preparing the composites of SnO_2/CN_xNTs and CeO_2/CN_xNTs without further purification because of the CoMo-300 product's low catalyst content. The inset shows the TEM images of the CN_xNTs of CoMo-300. It is clearly seen that the diameters of bamboo-like CN_xNTs are 20–30 nm, and the bamboo-like structure is the representative feature of CN_xNTs which consists of uniform and well-ordered compartments in contrast to the straight CNTs [26].

The morphology of the CN_xNTs composites was observed via SEM. Fig. 2(a and d) shows that the SnO_2/CN_xNTs and CeO_2/CN_xNTs composites have one-dimensional nanostructures with uniform diameter ranging from 20 to 30 nm. The surface of the CN_xNTs is not smooth, and it is shown that plenty of SnO_2 and CeO_2 nanoparticles were anchored on the surface of CN_xNTs.

The TEM images of Fig. 2(b and e) show that the SnO_2 and CeO_2 nanoparticles anchored on the surface of CN_xNTs successfully. The insets are the particle diameter histograms of the SnO_2 and CeO_2 nanoparticles on the surface of CN_xNTs obtained from the TEM images. The diameters of SnO_2 and CeO_2 particles are at an average size of 3.5 ± 1 nm and 5.5 ± 1.5 nm, respectively. Fig. 2(c) shows the clear (1 1 0) and (1 0 1) lattice fringes of SnO_2 with the interplanar spacing of 0.336 nm and 0.265 nm. Fig. 2(f) shows the clear (1 1 1) and (2 0 0) lattice fringes of CeO_2 with the interplanar spacing of 0.320 and 0.270 nm, respectively. And it also reveals that CN_xNTs have the interlayer distance of 0.35 nm compared with pure CNTs (0.34 nm). It is possibly due to the doped nitrogen atom deforming the framework of CN_xNTs.

Fig. 3(a) is the XPS spectrum of Sn 3d scan of SnO_2/CN_xNTs. The dominant signals corresponding to Sn $3d_{5/2}$ and Sn $3d_{3/2}$ were found at 486.4 eV and 494.8 eV as the Sn (IV) oxidation state which agree with the report for SnO_2 [27]. From the spectrum of Fig. 3(b), it can be seen that the Ce $3d_{5/2}$ and Ce $3d_{3/2}$ peaks exist mainly as the Ce (IV) oxidation state (882.8 eV and 900.9 eV), other peaks are shoulder peaks. The results are consistent with the report [28] and the HRTEM analysis in Fig. 2. In order to study the interaction between the nitrogen atoms and the metallic oxide (SnO_2 and CeO_2) nanoparticles, the N 1s XPS spectra of CN_xNTs and SnO_2/CN_xNTs and CeO_2/CN_xNTs were investigated. Fig. 3(c) shows that each XPS spectrum of N 1s scan is composed of four peaks, which are around 398.7, 401.0, 404.3 and 407.0 eV, respectively. P1 (398.7 eV) can be assigned to the pyridine-like N; P2 (401.0 eV)

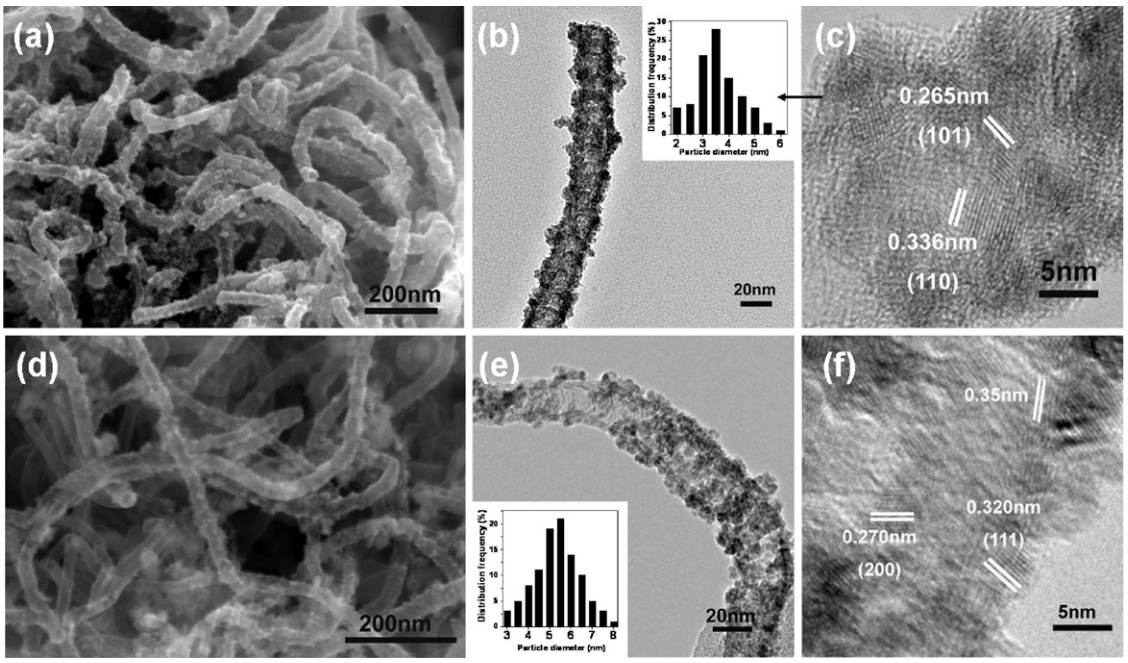

Fig. 2. (a, d) SEM and (b, e) TEM images (the inset shows the particle diameter histogram of the sample) of SnO_2/CN_xNTs and CeO_2/CN_xNTs. (c, f) HRTEM images of SnO_2/CN_xNTs and CeO_2/CN_xNTs.

can be assigned to graphite-like N; the higher binding energy of P3 and P4 (404–408 eV) can be assigned to molecular N_2 and nitrogen oxides adsorbed on the surface of the CN_xNTs [29,30]. It is known to all that just the pyridine-like N and the graphite-like N are embedded in the skeleton of CN_xNTs, and it is obviously shown that the amount of graphite-like N is more than that of pyridine-like N in the framework of CN_xNTs (see Table 1).

The binding energy of P1 of SnO_2/CN_xNTs and CeO_2/CN_xNTs composites is around 398.3 eV, in comparison to the P1 of CN_xNTs (398.7 eV), there is 0.4 eV shift of the P1 peak, and for the binding energy of P2, it also existes 0.3 or 0.1 eV shift. As it is known, the electronegativity of nitrogen (2.8–3.4) is stronger than those of tin (1.8) and cerium (1.1–1.2), if tin or cerium atom interacts with nitrogen atom, the nitrogen atom may strongly absorb the electron of tin or cerium atom so that the binding energy of N 1s will reduce. It corresponds to the spectra Fig. 3(c). This demonstrates that there exists strongly interaction between the metallic oxide (SnO_2 and CeO_2) nanoparticles and the N atoms (pyridine-like N and graphite-like N) of CN_xNTs.

Table 1
The atomic concentration of various doped N types and total N (N_{total}) in CN_xNTs, SnO_2/CN_xNTs and CeO_2/CN_xNTs.

Samples	Pyridine-like N (at. %)[a]	Graphite-like N (at. %)[b]	Other N (at. %)[c]	N_{total} (at. %)
CN_xNTs	1.52	2.89	0.93	5.34
SnO_2/CN_xNTs	0.97	2.68	1.04	4.52
CeO_2/CN_xNTs	0.89	2.59	0.84	4.32

[a] A1 (%) × N_{total} (at. %).
[b] A2 (%) × N_{total} (at. %).
[c] (A3+A4) (%) × N_{total} (at. %). A1, A2, A3 and A4 are the area % of P1, P2, P3 and P4 peaks.

As shown in Table 1, the nitrogen atomic concentration of SnO_2/CN_xNTs and CeO_2/CN_xNTs are both around 5.34 at. %. It is one

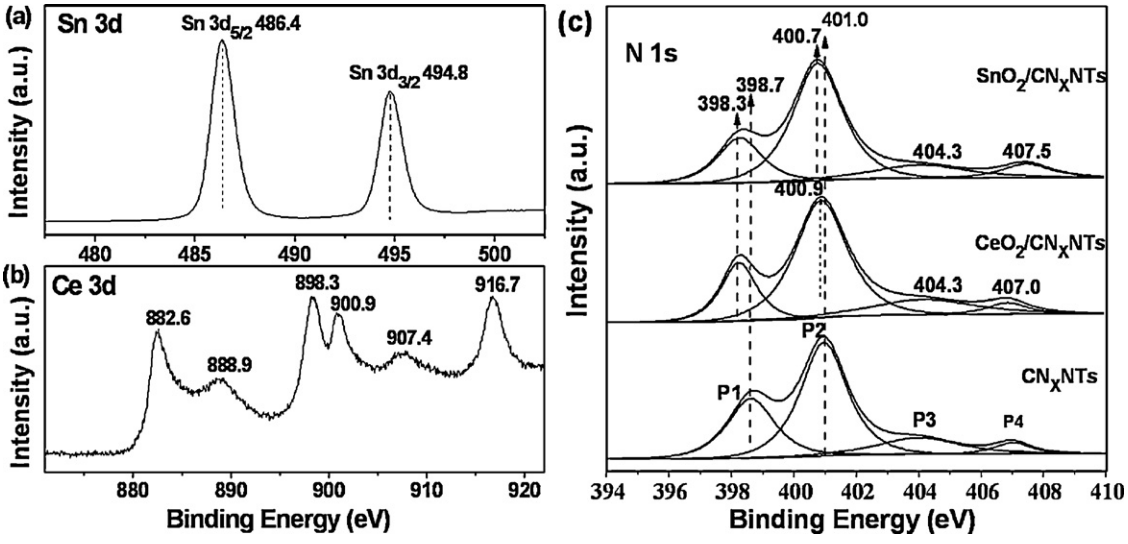

Fig. 3. XPS spectra of (a) Sn 3d scan of SnO_2/CN_xNTs, (b) Ce 3d scan of CeO_2/CN_xNTs and (c) N 1s scan of CN_xNTs, SnO_2/CN_xNTs and CeO_2/CN_xNTs.

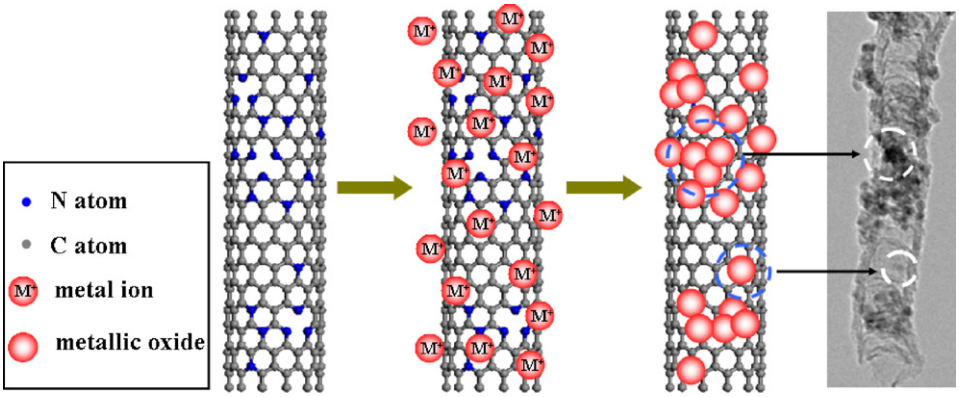

Fig. 4. Schematic diagram of the composite process.

desired ratio which demonstrates that more nitrogen atoms doped into the framework of the CNTs. The nitrogen atoms play the role of activity point on the surface of CN_xNTs. At this ratio, more SnO_2 and CeO_2 could anchor on the surface of CN_xNTs due to more activity point. And in this table, the composites of SnO_2/CN_xNTs and CeO_2/CN_xNTs have lower pyridine-like N content than the pristine CN_xNTs, this problem attributes to the aggregation of SnO_2 and CeO_2 nanoparticles grown at the pyridine-like N, and the thick packs covered the pyridine-like N.

According to the above analysis, the formation mechanism of SnO_2/CN_xNTs or CeO_2/CN_xNTs was put forward in Fig. 4. Without acid treatment of the CN_xNTs, metal ion (Sn^{2+} or Ce^{3+}) could easily adsorbed on the pyridine-like N and the graphite-like N of the CN_xNTs, since the electron densities of the pyridine-like N and the graphite-like N are higher than that of the C atoms in CN_xNTs, the nitrogen atoms which have extra electron substituted for carbon atoms in the framework of CN_xNTs, thus, the extra electrons of CN_xNTs have similar role to the negative electricity group, such as –COOH, on the surface of CNTs after acid treatment. When adding the CN_xNTs into the aqueous solution of $SnCl_2$ or $Ce(NO_3)_3$, the Sn^{2+} or the Ce^{3+} ion carried positive electricity might move and adsorb to the negative electricity activity site of the nitrogen atoms.

The pyridine-like N corresponds to the N atoms occupying the vacancy formed by removing a central C atom among three hexagons and replacing the three surrounding C atoms with three N atoms [31,32]. And the pyridine-like N has two extra nonbonding electrons in its sp^2-hybridized orbital, acting as a nonbonding p-orbital. Therefore, the three pyridine-like N atoms will form a strongly negative electricity centre which offers higher stability to form heterojunction between CN_xNTs and metal oxide. In addition, compared with the pyridine-like N, the graphite-like N corresponds to the N atoms substituting for C atoms in the graphite layers without forming a vacancy, the graphite-like N can also absorb metal oxide. According to the XPS results, there are the peak shifts of both the pyridine-like N and the graphite-like N structures of the SnO_2/CN_xNTs and CeO_2/CN_xNTs composites, compared with the pristine CN_xNTs. It can be concluded that the metal ions can be anchored at the sites of the pyridine-like N and the graphite-like N of CN_xNTs.

Fig. 5(a) shows the CV results of the CN_xNTs of CoMo-300 (without purification and after purification by hydrochloric acid) modified electrodes in the PBS solution saturated with NO. The two curves show the extremely similar feature, and the obvious oxidation peaks indicate that both of the CN_xNTs without purification and after purification have excellent electrooxidation for NO. So the CN_xNTs of CoMo-300 with high yield were employed to composite with SnO_2 and CeO_2 nanoparticles directly without removing the catalyst residue because the catalyst impurities have little effect on the electrochemistry performance.

Fig. 5(b) shows the CV results of SnO_2/CN_xNTs, CeO_2/CN_xNTs, CN_xNTs, SnO_2/CNTs, CNTs, CeO_2/CNTs, SnO_2 and CeO_2 modified electrodes in the PBS saturated with NO. In general, the higher the peak current density shows, the faster the reaction rate of NO electrooxidation is. For the CeO_2/CN_xNTs and SnO_2/CN_xNTs modified electrodes, the value of the peak current density is 17.65 and 11.81 mA/cm^2, respectively, which is much higher than that of other modified electrodes. The order of peak current density is: CeO_2/CN_xNTs > SnO_2/CN_xNTs > CN_xNTs > SnO_2/CNTs > CNTs > CeO_2/CNTs > SnO_2 > CeO_2. The CeO_2/CN_xNTs and SnO_2/CN_xNTs compos-

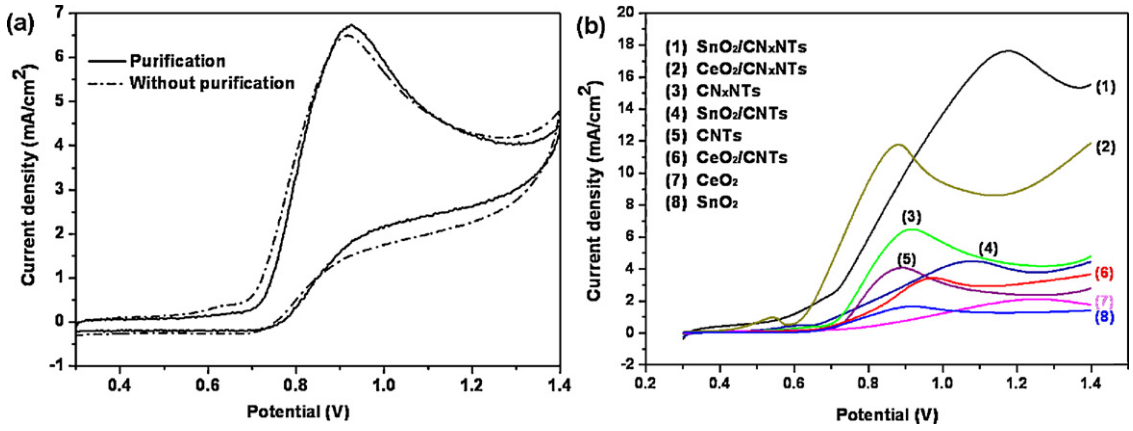

Fig. 5. (a) CV curves of the CN_xNTs of CoMo-300 (without purification and after purification) modified electrodes in the PBS saturated with NO. (b) CV curves of samples (1–8) modified electrodes in the PBS saturated with NO. The scan rate above was 0.01 V/s.

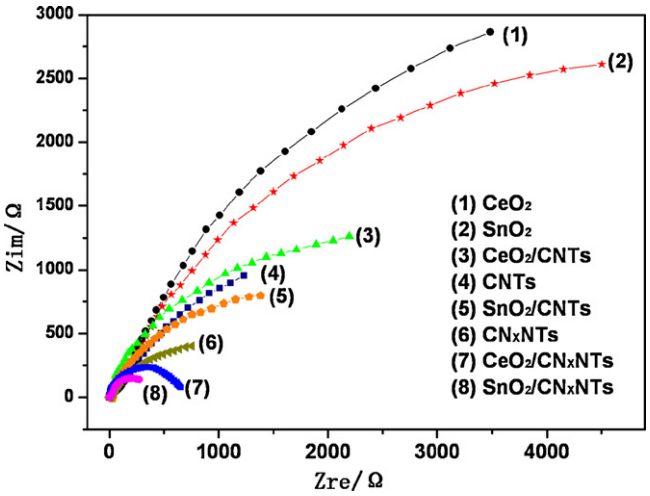

Fig. 6. Nyquist plots of samples (1–8) modified electrodes in PBS saturated NO (potential: 0.70 V).

Table 2
The values of peak potential, current density and charge transfer resistance (R_{ct}) for NO electrooxidation.

Modified electrode	NO electrooxidation peak		R_{ct} (Ω)
	Potential (V)	Current density (mA/cm^2)	
SnO_2/CN_xNTs	1.16	17.65	407
CeO_2/CN_xNTs	0.88	11.81	686
CN_xNTs	0.92	6.55	2259
SnO_2/CNTs	1.08	4.44	3690
CNTs	0.89	4.09	5012
CeO_2/CNTs	0.98	3.46	6186
SnO_2	1.25	2.12	9830
CeO_2	0.92	1.77	12262

ites show much higher peak current density than CN_xNTs and SnO_2 (or CeO_2) nanoparticles. Comparing with other obtained CNTs composites, just the SnO_2/CNTs composites show a little enhancement to CNTs, the peak current density of CeO_2/CNTs is even lower than that of CNTs. The CV results indicate that CN_xNTs-based composites show preferable performance for NO electrooxidation compared with conventional CNTs-based composites. This result is attributed to the improved electrical conductivity of CN_xNTs and the strong interaction between CN_xNT and SnO_2 (or CeO_2) which has discussed above [33].

Fig. 6 shows the Nyquist plots of CeO_2, SnO_2, CeO_2/CNTs, CNTs, SnO_2/CNTs, CN_xNTs, CeO_2/CN_xNTs and SnO_2/CN_xNTs modified electrodes in the PBS saturated with NO at the potential of 0.70 V. Here, EIS was employed to investigate NO electrooxidation at different modified electrodes. The used AC voltage amplitude was 0.01 V in the frequency range from 1 Hz to 100 kHz. The resistance values of charge transfer were calculated by Zview2 software. As shown in Fig. 6 and Table 2, there are big capacitive semicircles of CeO_2 and SnO_2 modified electrodes, and the capacitive semicircles of the SnO_2/CN_xNTs and CeO_2/CN_xNTs modified electrodes are small. The value of charge transfer resistance (R_{ct}) of CeO_2, SnO_2, CeO_2/CNTs, CNTs, SnO_2/CNTs, CN_xNTs, CeO_2/CN_xNTs and SnO_2/CN_xNTs modified electrodes are shown in Table 2. It is known that the lower R_{ct} of the modified electrode corresponds to the faster rate of charge transfer. The order of charge transfer rate is: CeO_2/CN_xNTs > SnO_2/CN_xNTs > CN_xNTs > SnO_2/CNTs > CNTs > CeO_2/CNTs > SnO_2 > CeO_2, and the results are consistent with the CV measurements. All of the above facts demonstrate that the CN_xNTs-based composites have excellent performance for NO electrooxidation compared with the conventional CNTs-based composites.

4. Conclusions

CN_xNTs with high yield and desired nitrogen content have been fabricated via a feasible method. Then, SnO_2/CN_xNTs and CeO_2/CN_xNTs composites have been successfully prepared due to the inherent surface activity of CN_xNTs without any pre-treatment. The CN_xNTs-based composites as electrode materials show better electrocatalytic activity for NO electrooxidation than the conventional CNTs-based composites according to cyclic voltammetry results, indicating their potential application in electrochemistry sensor for NO. Apparently, this efficient strategy for preparing CN_xNTs-based composites could be further extended to modify other metal and metal oxide nanoparticles on the surface of CN_xNTs, such as Pt, Ni, TiO_2 and NiO, with applications in catalysis, sensors and batteries.

Acknowledgments

This work was supported by the National Natural Science Foundation of China (no. 21076066) and the Key Projects of the Natural Science Foundation of Heilongjiang province (no. ZD201002).

References

[1] K. Xiao, Y.Q. Liu, P.A. Hu, G. Yu, Y.M. Sun, D.B. Zhu, J. Am. Chem. Soc. 127 (2005) 8614.
[2] Y. Chai, X.L. Zhou, P.J. Li, W.J. Zhang, Q.F. Zhang, J.L. Wu, Nanotechnology 16 (2005) 2134.
[3] P.X. Hou, S.T. Xu, Z. Ying, Q.H. Yang, C. Liu, H.M. Cheng, Carbon 41 (2003) 2471.
[4] F. Lamari Darkrim, P. Malbrunot, G.P. Tartaglia, Int. J. Hydrogen Energy 27 (2002) 193.
[5] K.P. Gong, F. Du, Z.H. Xia, M. Durstock, L.M. Dai, Science 323 (2009) 760.
[6] G.P. Jin, R. Baron, N.V. Rees, L. Xiao, R.G. Compton, New J. Chem. 33 (2009) 107.
[7] W. Cha, M.E. Meyerhoff, Langmuir 220 (2006) 10830.
[8] A. Yang, X.M. Tao, R.X. Wang, Appl. Phys. Lett. 91 (2007) 133110.
[9] X.G. Hu, T. Wang, X.H. Qu, S.J. Dong, J. Phys. Chem. B 110 (2006) 853.
[10] C. Wan, R.T. Lv, F.Y. Kang, J.L. Gu, X.C. Gui, D.H. Wu, J. Magn. Magn. Mater. 321 (2009) 1924.
[11] D. Eder, Chem. Rev. 110 (2010) 1348.
[12] N. Kakati, J. Maiti, S.H. Jee, S.H. Lee, Y.S. Yoon, J. Alloys Compd. 509 (2011) 5617.
[13] P.Y. Keng, B.Y. Kim, I.B. Shim, R. Sahoo, P.E. Veneman, N.R. Armstrong, H. Yoo, J.E. Pemberton, M.M. Bull, J.J. Griebel, E.L. Ratcliff, K.G. Nebesny, J. Pyun, ACS Nano 3 (2009) 3143.
[14] D. Abdula, M. Shim, ACS Nano 2 (2008) 2154.
[15] B.G. Wei, L.Y. Zhang, G. Chen, New J. Chem. 34 (2010) 453.
[16] R. Czerw, M. Terrones, J.C. Charlier, X. Blase, B. Foley, R. Kamalakaran, N. Grobert, H. Terrones, D. Tekleab, P.M. Ajayan, W. Blau, M. Ruhle, D.L. Carroll, Nano Lett. 1 (2001) 457.
[17] Z.J. Wang, R.R. Jia, J.F. Zheng, J.H. Zhao, L. Li, J.L. Song, Z.P. Zhu, ACS Nano 5 (2011) 1677.
[18] X.Y. Tao, X.B. Zhang, F.Y. Su, J.P. Cheng, F. Liu, Z.Q. Luo, Diam. Relat. Mater. 16 (2007) 425.
[19] K. Ghosh, M. Kumar, H.F. Wang, T. Maruyama, Y. Ando, Langmuir 26 (2010) 5527.
[20] B. Yue, Y.W. Ma, H.S. Tao, L.S. Yu, G.Q. Jian, X.Z. Wang, X.S. Wang, Y.N. Lu, H. Zheng, J. Mater. Chem. 18 (2008) 1747.
[21] E.H. Espinosa, R. Ionescu, B. Chambon, G. Bedis, E. Sotter, C. Bittencourt, A. Felten, J.J. Pireaux, X. Correig, E. Llobet, Sens. Actuators B 127 (2007) 137.
[22] E. Topoglidis, Y. Astuti, F. Duriaux, M.G. tzel, J.R. Durrant, Langmuir 19 (2003) 6894.
[23] Z.L. Wu, M.J. Li, J. Howe, H.M. Meyer, S.H. Overbury, Langmuir 26 (2010) 16595.
[24] I. Atribak, A.B. Lopez, A.G. Garcia, B. Azambre, Phys. Chem. Chem. Phys. 12 (2010) 13770.
[25] K. Kan, T.L. Xia, L. Li, H.M. Bi, H.G. Fu, K.Y. Shi, Nanotechnology 20 (2009) 185502.
[26] B.L. Allen, M.B. Keddie, A. Star, Nanoscale 2 (2010) 1105.
[27] L.Y. Liang, Z.M. Liu, H.T. Cao, X.Q. Pan, ACS Appl. Mater. Interfaces 2 (2010) 1060.
[28] A. Gupta, M.S. Hegde, K.R. Priolkar, U.V. Waghmare, P.R. Sarode, S. Emura, Chem. Mater. 21 (2009) 5836.
[29] J. Amadou, K. Chizari, M. Houlle, I. Janowska, O. Ersen, D. Be'gin, C.P. Huu, Catal. Today 138 (2008) 62.
[30] S. Maldonado, S. Morin, K.J. Stevenson, Carbon 44 (2006) 1429.
[31] S.H. Lim, R.J. Li, W. Ji, J.Y. Lin, Phys. Rev. B 76 (2007) 195406.
[32] W.X. Lv, K.Y. Shi, L. Li, S.Z. Shao, Microchim Acta 170 (2010) 91.
[33] G. Vijayaraghavan, K.J. Stevenson, Langmuir 23 (2007) 5279.